BRAIN COMMUNICATIONS

Amyloid-driven disruption of default mode network connectivity in cognitively healthy individuals

Silvia Ingala,[1] Jori Tomassen,[2] Lyduine E. Collij,[1] Naomi Prent,[2,3,4] Dennis van 't Ent,[5] Mara ten Kate,[1,2] Elles Konijnenberg,[2] Maqsood Yaqub,[1] Philip Scheltens,[2] Eco J.C. de Geus,[5] Charlotte E. Teunissen,[6] Betty Tijms,[2] Alle Meije Wink,[1] Frederik Barkhof,[1,7] Bart N.M. van Berckel,[1] Pieter Jelle Visser[2] and Anouk den Braber[2,5]

Cortical accumulation of amyloid beta is one of the first events of Alzheimer's disease pathophysiology, and has been suggested to follow a consistent spatiotemporal ordering, starting in the posterior cingulate cortex, precuneus and medio-orbitofrontal cortex. These regions overlap with those of the default mode network, a brain network also involved in memory functions. Aberrant default mode network functional connectivity and higher network sparsity have been reported in prodromal and clinical Alzheimer's disease. We investigated the association between amyloid burden and default mode network connectivity in the preclinical stage of Alzheimer's disease and its association with longitudinal memory decline. We included 173 participants, in which amyloid burden was assessed both in CSF by the amyloid beta 42/40 ratio, capturing the soluble part of amyloid pathology, and in dynamic PET scans calculating the non-displaceable binding potential in early-stage regions. The default mode network was identified with resting-state functional MRI. Then, we calculated functional connectivity in the default mode network, derived from independent component analysis, and eigenvector centrality, a graph measure recursively defining important nodes on the base of their connection with other important nodes. Memory was tested at baseline, 2- and 4-year follow-up. We demonstrated that higher amyloid burden as measured by both CSF amyloid beta 42/40 ratio and non-displaceable binding potential in the posterior cingulate cortex was associated with lower functional connectivity in the default mode network. The association between amyloid burden (CSF and non-displaceable binding potential in the posterior cingulate cortex) and aberrant default mode network connectivity was confirmed at the voxel level with both functional connectivity and eigenvector centrality measures, and it was driven by voxel clusters localized in the precuneus, cingulate, angular and left middle temporal gyri. Moreover, we demonstrated that functional connectivity in the default mode network predicts longitudinal memory decline synergistically with regional amyloid burden, as measured by non-displaceable binding potential in the posterior cingulate cortex. Taken together, these results suggest that early amyloid beta deposition is associated with aberrant default mode network connectivity in cognitively healthy individuals and that default mode network connectivity markers can be used to identify subjects at risk of memory decline.

1 Department of Radiology and Nuclear Medicine, Amsterdam Neuroscience, Vrije Universiteit Amsterdam, Amsterdam UMC, Location VUmc, 1081 HZ Amsterdam, The Netherlands
2 Alzheimer Center Amsterdam, Department of Neurology, Amsterdam Neuroscience, Vrije Universiteit Amsterdam, Amsterdam UMC, Location VUmc, 1081 HZ Amsterdam, The Netherlands
3 Faculty of Behavioral and Movement Sciences, Section Clinical Neuropsychology, Vrije Universiteit Amsterdam, 1081 HV Amsterdam, The Netherlands
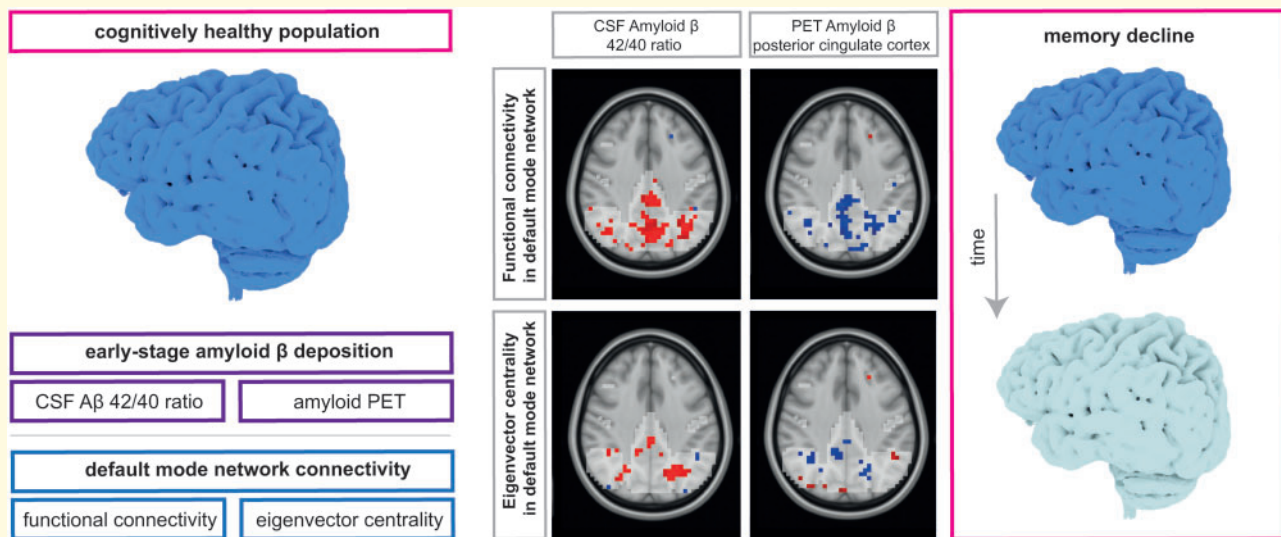4 Vesalius, Centre for Neuropsychiatry, GGZ Altrecht, 3447 GM Woerden, The Netherlands

5   Department of Biological Psychology, Vrije Universiteit Amsterdam, Neuroscience Amsterdam, 1081 HV Amsterdam, The Netherlands
6   Department of Clinical Chemistry, Neurochemistry Laboratory, Vrije Universiteit Amsterdam, Amsterdam Neuroscience, Amsterdam UMC, 1081 HV Amsterdam, The Netherlands
7   Institute of Neurology and Healthcare Engineering, University College London, WC1E 6BT London, UK

Correspondence to: Silvia Ingala
Department of Radiology and Nuclear Medicine
Amsterdam UMC—Location Vumc, PO Box 7057, 1007 MB Amsterdam, The Netherlands
E-mail: s.ingala@amsterdamumc.nl

Graphical Abstract

Introduction

Cortical amyloid beta ($A\beta$) accumulation seems to be the first event of Alzheimer's disease pathophysiological cascade and can be detected indirectly in CSF[1] or directly through the visualization of $A\beta$ fibrils on PET scans.[2,3] It has been reported that CSF analysis is more sensitive than global amyloid PET in early Alzheimer's disease stages,[4] capturing the soluble part of amyloid pathology, crucial in the origin of synaptic pathology.[5,6] Nevertheless, recent evidence suggests that $A\beta$ deposition follows a consistent spatio-temporal order across the brain, making regional PET suitable for visualization of early Alzheimer's disease pathology.[7,8] Early $A\beta$-accumulating regions correspond to the posterior cingulate (PCC), precuneus and medial orbitofrontal (MOF) cortex.[7–9] Such regions largely overlap with a functional brain network called the default mode network (DMN).[9–13] It has been proposed that

DMN disruptions might represent one of the early functional consequences associated with the molecular pathological processes underlying Alzheimer's disease.[3,10] Nonetheless, while aberrant DMN connectivity in Alzheimer's dementia has been reported,[14] studies investigating earlier stages of the Alzheimer's disease continuum show conflicting results.[3,9,15–17]

DMN areas show synchronous activity at resting-state functional magnetic resonance imaging (rs-fMRI) when an individual is awake but not involved in any specific mental activity.[18,19] This is indirectly measured with independent component analysis (ICA) of blood oxygen level dependent (BOLD) signal, where local BOLD variability is interpreted as a proxy for variations in local neuronal activity and rs-fMRI functional connections are measured as synchronized BOLD signal variability between different brain regions in the absence of a task.[20] The degree of co-activation of the network can be derived through

dual-regression and defined as functional connectivity (FC).[21] Brain FC has been proposed to reflect the extent of neuronal metabolic activity.[22] To elucidate further connectivity within the DMN, graph theoretical methods might be used.[23] Specifically, eigenvector centrality (EC) reflects layers in the hierarchy of a network, recursively defining important nodes as those having more connections with other important nodes.[24,25] EC might therefore be useful in localizing prominent hubs within the DMN through a hypothesis-free, data-driven method.[25]

Regions of the DMN have been involved in memory retrieval,[26] frequently impaired in Alzheimer's disease individuals.[18] An extensive body of literature identified memory as one of the earliest and most severely affected cognitive domains in Alzheimer's disease.[27,28] In line with this, we recently showed that amyloid pathology, measured with both CSF Aβ 42/40 ratio and PET binding potential, is associated with memory dysfunction in elderly cognitively healthy individuals,[29] an association that was previously shown in later stages of Alzheimer's disease.[30,31]

With this in mind, we investigated whether early Aβ deposition, as defined both by CSF Aβ 42/40 ratio and PET [^{18}F]flutemetamol non-displaceable binding potential (BP$_{ND}$) in early-stage regions, is associated with abnormal FC and EC within the DMN in a cohort of elderly cognitively intact individuals.[32] As areas of the DMN are involved in memory circuits, and considering the association that we previously found between Aβ deposition and memory decline, we investigated whether FC within the DMN modifies the strength of this relation.

Materials and methods

Study participants

Study participants were selected from the European Information Framework for Alzheimer's Disease (EMIF-AD)-PreclinAD study.[32] Inclusion criteria were the following: age between 60 and 100, normal cognition as assessed by a delayed recall score > -1.5 SD of demographically adjusted normative data on the Consortium to Establish a Registry for Alzheimer's Disease 10 word list,[33] a Telephone Interview for Cognitive Status modified score ≥ 23,[34] a 15-item Geriatric Depression Scale score of < 11[35] and a Clinical Dementia Rating score of 0.[36] Individuals were excluded if they presented any significant medical, neurological or psychiatric condition potentially affecting cognitive performance or MRI contraindications. A total of 204 subjects were included in the EMIF-AD PreclinAD study. A subset of 190 subjects had both T$_1$-weighted and rs-fMRI scans available. Seventeen individuals were excluded due to lack of sufficient good-quality images, resulting in a total of 173 individuals. We defined amyloid status using either visual read of dynamic [^{18}F]flutemetamol PET images or CSF

Aβ42/40 ratio (ADx Neurosciences/Euroimmun assays) <0.066 (based on Gaussian mixture modelling).

Neuropsychological assessment

Longitudinal neuropsychological data were retrieved at two follow-up time points for subsets of 165 and 94 participants respectively (mean follow-up 1 duration 23 ± 3 months; mean follow-up 2 duration 50 ± 3 months; mean difference between follow-up time points 26 ± 2 months). Our sample comprised cognitively healthy individuals, thus detecting incipient cognitive dysfunction was not trivial. In light of this, we chose to focus on the memory domain as lower memory was previously associated with higher Aβ in this cohort.[29] We generated baseline and follow-up memory composite scores by using the total immediate recall and delayed recall of the Dutch version of the Rey Auditory Verbal Learning test (RAVLT),[37,38] the 3- and 20-minute recall of the Rey Complex Figure (RCF),[39,40] the total score from the Face Name Associated Memory Examination (FNAME)-names and occupations delayed recall.[41,42] Composite scores were only computed for participants with at least four test scores. All test scores were z-transformed using the baseline mean and standard deviation of the total sample (N$_{\text{EMIF-AD PreclinAD}}$ = 204), and combined into one composite score. Memory slopes were calculated as the difference between follow-up and baseline composite scores, divided by time between measurements.

Cerebrospinal fluid

Lumbar puncture was performed between 10 AM and 2 PM, after at least 2 h of fasting, using Sarstedt polypropylene syringes and a Spinocan 25 Gauge needle. Up to 20 mL CSF was obtained from 109 (63%) study participants. CSF samples were centrifuged at 1300–2000 g at 4°C for 10 min and supernatants were stored in Sarstedt aliquots of 0.5 mL at −80°C until analysis. A maximum of 2 h was allowed between lumbar puncture and freezing.[43] Aβ 42/40 ratio levels were analysed at the Neurochemistry Laboratorium of the Amsterdam UMC by personnel blinded to clinical information using ADx Neurosciences/Euroimmun kits from the same batch, according to the manufacturer instructions.[44,45]

MRI and PET acquisition

Whole-brain MRI and PET scans were acquired at Amsterdam University Medical Center, location VUmc, using a 3 T Philips Ingenuity Time-of-Flight PET/MRI scanner (Philips Healthcare, Cleveland, USA) with an 8-channel head coil.

High-resolution isotropic structural 3D T$_1$-weighted images were acquired using a sagittal turbo field echo sequence (1.00 mm^3 isotropic voxels, repetition time = 7.9 ms, echo time = 4.5 ms and flip angle = 8°). Whole brain rs-fMRI scans were acquired using a fast field

echo-planar imaging (EPI) sequence (repetition time (TR) = 1800 ms; echo time (TE) = 35 ms; flip angle (FA) = 80°; matrix = 64 × 64; field of view (FOV) = 221 mm; voxel size = 3.3 mm × 3.3 mm × 3.0 mm). In total, 33 axial AP-oriented slices were acquired in interleaved order, resulting in a total of 202 volumes. During the rs-fMRI scan, light and music were turned off and participants were instructed to keep their eyes closed, remain awake, and not think to anything in particular. All MRI scans were visually assessed by an experienced neuroradiologist for incidental findings.

Dynamic [^{18}F]flutemetamol amyloid-PET scans were performed according to a dual-time window acquisition protocol[46] with 30 min scans acquired immediately after manual tracer injection (dose: 191 ± 20 MBq), followed by a 60 min break, and then a second scan of 20 min (*i.e.* 90–110 min post injection) (for further details see Konijnenberg *et al.*[32]). A 3D T$_1$-weighted gradient echo pulse MR image was acquired prior to each PET scan for attenuation correction.

MRI analysis

Grey matter (GM) volume, normalized for head size, was estimated using SIENAX,[47] part of FMRIB's Software Library (FSL Version 5.0.4; www.fmrib.ox.ac.uk/fsl Accessed 15 September 2021).[48]

Preprocessing of rs-fMRI scans was also performed using the FSL pipeline (FSL Version 5.0.4; www.fmrib.ox.ac.uk/fsl Accessed 15 September 2021)[48] and it consisted of motion correction,[49] removal of non-brain tissue,[50,51] spatial smoothing by using a Gaussian kernel of 5 mm full width at half maximum (FWHM) to reduce noise, and high-pass temporal filtering to remove low-frequency artefacts. After preprocessing, affine registration[49] was used to register rs-fMRI images to 3D T$_1$-weighted images. Subsequently, the images were registered to Montreal Neurological Institute (MNI) standard space images using nonlinear registration (FNIRT) with a warp resolution of 10 mm and resampling resolution of 4 mm. ICA of rs-fMRI data was performed using FSL MELODIC to decompose functional images into independent, uncorrelated spatial and temporal components,[48,52] automatically estimating the number of components, which was 38. We identified the DMN as the component that showed the highest spatial correlation with the previously defined rs-fMRI DMN map by Smith *et al.*[53] To identify individual differences in DMN FC with spatial maps from the group-average ICA, dual regression was performed[54] (Fig. 1).

The dual regression method[55] regresses an fMRI dataset onto a set of spatial patterns indicating a possible resting state network, resulting in a representative time series per pattern, per subject. After that, the fMRI data are regressed onto these representative time series, yielding a voxelwise measure of temporal correspondence with

each pattern, for each subject. Both steps are generalized linear models for data $Y_{[N \times T]}$ of N voxels and T time points and a set $C_{[N \times M]}$ of M spatial patterns. The first step solves the following equation:

$$Y_{[N \times T]} = C_{[N \times M]} \times S_{[M \times T]} + \mathcal{E}_{[N \times T]}$$

for the pattern-specific time series S (with residual ε), and the second step solves the formula

$$Y_{[N \times T]} = D_{[N \times M]} \times S_{[M \times T]} + \mathcal{E}_{[N \times T]}$$

for the voxelwise correspondence D to S, and can be computed with a least squares method. The output of the dual regression method, first introduced in 2009,[54] has been used to identify between-group resting state network differences.[55,56]

Voxelwise functional network centrality can be defined as the local proportional relevance to the whole-brain pattern of synchronized activity.[57] Eigenvector centrality mapping (ECM) uses the coefficients of the dominant eigenvector of the fMRI connectivity matrix and is highest for voxels that have strong correlations with other central voxels.[58] ECM was performed using fastECM,[24] an efficient implementation of ECM using power iteration. ECM computations used the standard-space fMRI data as described above and were performed inside a mask where 75% of the participants had BOLD measurements during the whole time series, to balance brain coverage and preservation of network topology. EC values inside the previously defined DMN mask were computed (Fig. 1).

ICA and EC methods have been chosen as they give voxelwise reports and they are robust against multiple sources of variability in resting-state fMRI analyses.[20,25]

PET analysis

PET scans were reconstructed by applying the LOR-RAMLA dedicated Philips reconstruction algorithm for the brain. The first emission scans were reconstructed into 18 frames with increasing time length (6 × 5, 3 × 10, 4 × 60, 2 × 150, 2 × 300, 1 × 600 s), while the second scan was reconstructed into 4 frames of 300 s each. Obtained PET images were preprocessed with Vinci Software version 2.56 (http://vinci.sf.mpg.de/ Accessed 15 September 2021). using its multimodality setting of Vinci for co-registration of dynamic scans with individual's T$_1$-weighted MRI sequences. Regions of interest (ROIs) were automatically delineated based on the T$_1$-weighted MRI images using PVElab.[59,60] Parametric non-displaceable binding potential (BP$_{ND}$) was calculated by using the receptor parametric mapping (RPM) implementation of the Simplified Reference Tissue Model (SRTM) in PPET.[46,61,62] Cerebellar GM was chosen as the reference region. For analyses, distribution volume ratio (DVR) was calculated as a measure of receptor availability for radioligand (BP$_{ND}$ + 1) and ROIs identified using Desikan–Killiani atlas.[63]
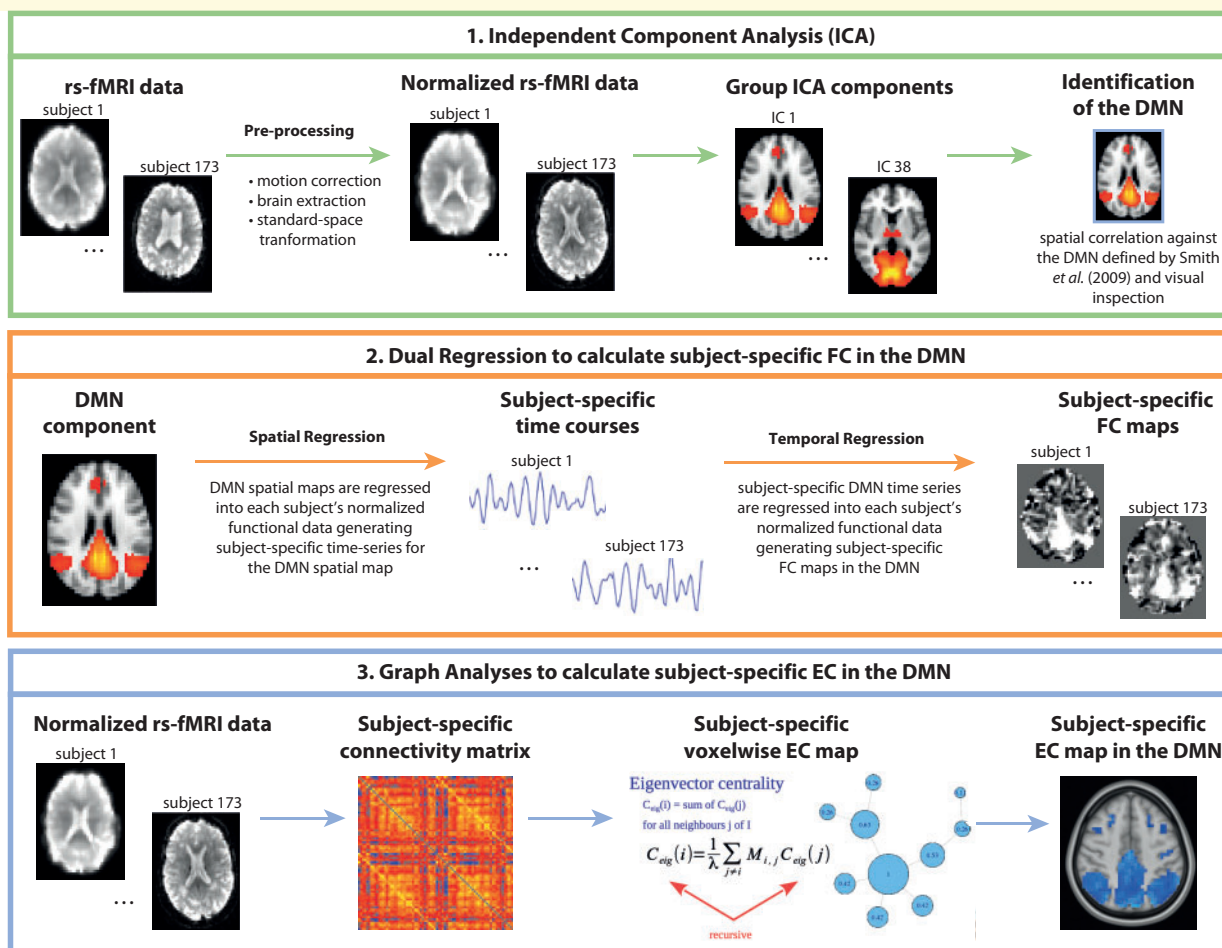
Figure 1. Overview of rs-fMRI data analyses. DMN, default-mode network; EC, eigenvector centrality; FC, functional connectivity; ICA, independent component analysis.

Statistical analyses

Each 3D subject-specific DMN connectivity map, resulting from dual regression, was averaged inside the mask of their corresponding DMN. FC values in each subject's DMN had been log-transformed to correct for a skewness in their distribution. Resulting output were mean FC and voxelwise FC within the DMN per subject, which were then used for statistical analyses.

Aß was used as a continuous measure and was defined as CSF Aß 42/40 ratio or PET BP_{ND} in early-stage Alzheimer's disease regions, *i.e.* the PCC, precuneus, and MOF cortex. Aß, log FC and normalized GM volume values were transformed to z-scores.

Four models tested the relationship between Aß burden and average FC in the DMN; one for each quantitative measure of Aß. We used generalized estimating equations (GEE), using family ID (indication of twin pairs) as a random factor, to correct for correlated observations in monozygotic twins,[64] and including age, sex and normalized GM volume as covariates.

To gain additional information on the effect of Aß on DMN FC and EC, a voxelwise GEE analysis was performed in the DMN mask voxels, correcting for the familial clustering of twin pairs, as well as confounders, such as age, sex and normalized GM volume. Of the clusters of voxels with *P-value* < 0.05, we selected the clusters with a minimum cluster extent of 10 voxels. To elucidate the role of FC in relation to memory decline, we tested whether FC in the DMN at baseline was predictive of longitudinal memory decline using GEE, correcting for age at the time of examination, sex, years of education, and using family ID as a random factor. Furthermore, given the known relationship between Aβ deposition and memory decline,[65,66] we also built a three-way interaction model which also included Aβ burden. All the statistical analyses were conducted in R version 3.6.0 (R Foundation for Statistical Computing, Vienna, Austria).

Data availability

Data requests can be submitted via the EMIF-AD Catalogue (see http://www.emif.eu/emif-ad-2/ Accessed 15 September 2021).

Results

Study sample

Demographics, clinical and imaging characteristics of the study participants are summarized in Table 1. The mean age of the population was 70.3 ± 7.4 years and the mini-mental state examination (MMSE) average was 29.0 ± 1.2, supporting that the population was cognitively unimpaired. CSF data were analysed for 109 out of the 173 study participants, while PET BP_{ND} could be estimated in a subset of 167 individuals. The amyloid burden was generally low, as expected in this cognitively normal cohort (amyloid positive, 17%). In line with the literature, amyloid positive individuals were generally older (*P*-value = 0.001) and had a slightly lower performance at neuropsychological tests (Table 1).

The results of follow-up memory tests are summarized in Table 2. On a group level, performance on RAVLT immediate and delayed recall decreased on follow-up. A learning effect was instead registered for the 3 min and 20 min RCF tests, and for the FNAME delayed recall subscores.

The relationship between amyloid burden and DMN connectivity

An inverse relationship was found between Aß burden and FC in the DMN when Aß was defined by CSF Aß 42/40 ratio (ß = 0.17, *P*-value = 0.020) and by PET BP_{ND} in the PCC (ß = −0.15, *P*-value = 0.006), but not with amyloid burden defined by PET BP_{ND} in the MOF and in the precuneus (MOF: ß = −0.09, *P*-value = 0.153; precuneus: ß = −0.09, *P*-value = 0.165) (Table 3).

We then investigated at a voxelwise level how FC and EC values within the DMN changed as a function of amyloid burden as defined by the amyloid metrics that showed a significant relationship between mean FC in the DMN, *i.e.* Aß 42/40 ratio and PET BP_{ND} in the PCC. Higher amyloid burden corresponded to lower FC and EC in voxels within the DMN, after correcting for age, sex, normalized GM volume and twin status (Table 4). Voxel clusters that significantly associated with early-stage Aβ pathology were localized in the precuneus, cingulate gyrus, and angular gyrus both for the FC and EC measures, and also in the middle cingulate gyrus for EC measures (Fig. 2).

The relationship between FC in the DMN and longitudinal memory decline

Next, we determined the impact that alterations in the DMN FC have on longitudinal memory decline through two-way and three-way interaction analyses. We found that baseline FC in the DMN was predictive of longitudinal memory decline independent of amyloid burden (Table 5). Moreover, our three-way interaction analysis showed a significant interaction between DMN FC and

Table 1 Description of the study participants at baseline.

	Total group (n = 173)	Amyloid negative (83%)	Amyloid positive (17%)	*P*-value
Demographics and clinical characteristics				
Age	70.3 ± 7.4	69.3	74.1	0.010
Sex, *n* females (%)	100 (57.8%)	78 (55.3%)	19 (65.5%)	0.421
Education (years)	11.6 ± 2.7	11.7 ± 2.6	11.1 ± 3.4	0.489
MMSE	29.0 ± 1.2	29.1 ± 1.1	28.6 ± 1.5	0.117
Neuropsychological tests				
RAVLT immediate recall (n = 164)	42.1 ± 9.0	42.8 ± 9.1	38.8 ± 7.8	0.06
RAVLT delayed recall (n = 164)	8.4 ± 2.8	8.5 ± 2.9	7.8 ± 2.2	0.112
RCF recall 3 min (n = 165)	18.8 ± 5.3	19.5 ± 5.3	15.6 ± 4.1	<0.001
RCF recall 20 min (n = 163)	18.7 ± 4.9	19.2 ± 4.8	16.0 ± 4.2	0.038
FNAME delayed recall subscore names (n = 150)	20.1 ± 9.9	21.0 ± 10.2	15.6 ± 6.7	0.397
FNAME delayed recall subscore occupation (n = 150)	33.2 ± 8.9	33.9 ± 8.8	29.8 ± 9.1	0.163
MRI imaging characteristics				
GM volume (cm^3)	72693 ± 8574	73260 ± 7403	72262 ± 4352	0.275
Log FC in the DMN	1.36 ± 0.14	1.36 ± 0.13	1.34 ± 0.13	0.209
Amyloid status				
CSF Aß 42/40 ratio (pg/ml) (n = 109)	0.10 ± 0.03	0.11 ± 0.02	0.05 ± 0.02	<0.001
PET Global DVR (n = 167)	1.03 ± 0.13	0.99 ± 0.08	1.20 ± 0.16	<0.001
PET DVR in the PCC (n = 167)	1.36 ± 0.19	1.30 ± 0.11	1.64 ± 0.24	<0.001
PET DVR in the precuneus (n = 167)	1.21 ± 0.16	1.17 ± 0.09	1.44 ± 0.22	<0.001
PET DVR in the MOF cortex (n = 167)	1.21 ± 0.18	1.15 ± 0.08	1.50 ± 0.23	<0.001

Data are presented as mean $\pm$ SD for continuous variables, or number (percentage) for dichotomous variables.
Aß, amyloid ß; DMN, default-mode network; DVR, distribution volume ratio; FC, functional connectivity, FNAME, face-name associated memory examination; GM, gray matter; MMSE, mini-mental state examination; MOF, medio-orbitofrontal cortex; PCC, posterior cingulate cortex; RAVLT, Rey auditory verbal learning test; RCF, Rey complex figure.

Table 2 Results of follow-up neuropsychological tests

Neuropsychological tests	Follow-up 1		Follow-up 2	
	N	Mean ± SD	N	Mean ± SD
RAVLT immediate recall	165	39.7 ± 9.1	93	43.6 ± 11.1
RAVLT delayed recall	165	7.7 ± 2.9	94	8.8 ± 3.4
RCF recall 3 min	164	19.7 ± 5.8	92	20.9 ± 5.7
RCF recall 20 min	164	19.7 ± 5.5	92	20.5 ± 5.6
FNAME delayed recall subscore names	154	21.5 ± 11.0	89	26.2 ± 10.8
FNAME delayed recall subscore occupation	154	33.4 ± 7.8	89	34.6 ± 8.9

FNAME, face-name associated memory examination; RAVLT, Rey auditory verbal learning test; RCF, Rey complex figure.

Table 3 Association of mean FC in the DMN and amyloid burden

	FC DMN Regression coefficient (β)	P-value
CSF Aβ 42/40 ratio	0.17	0.020
BP_{ND} in the PCC	−0.15	0.006
BP_{ND} in precuneus	−0.09	0.165
BP_{ND} in MOF cortex	−0.09	0.153

All values were transformed to z-scores. All GEE analyses took into account family ID as a random factor and were corrected for age, sex, and normalized GM volume.
Aβ, amyloid ß; BP_{ND}, non-displaceable binding potential; DVR, distribution volume ratio; MOF, medio-orbitofrontal cortex; PCC, posterior cingulate cortex; GEE, generalized estimating equations.

Aβ as defined by PET BP_{ND} in PCC (but not as CSF Aβ 42/40 ratio) in predicting longitudinal memory decline (interaction term PET BP_{ND} in PCC*FC in DMN*age: $\beta = -0.064$, P-value = 0.014) (Table 5).

Discussion

In this study, we investigated the relation between Aβ deposition and connectivity within the DMN in a cohort of cognitively healthy elderly individuals. We found that amyloid burden as defined by CSF Aβ 42/40 ratio and PET binding potential in the PCC is predictive of lower FC in the DMN. Furthermore, we showed that alterations of FC and EC measures as a function of Aβ deposition are strongest in voxel clusters localized in the precuneus, cingulate gyrus, angular gyrus and left middle temporal gyrus. Finally, we demonstrated that FC in the DMN is predictive of longitudinal memory decline, and its effect is synergistic with that of Aβ as defined by PET BP_{ND} in PCC.

This study demonstrates that early-stage Aβ accumulation as determined by regional PET amyloid deposition, namely in the PCC, is associated with aberrant DMN connectivity in a cognitively healthy population. We also show voxelwise FC and EC alterations in the DMN of early Aβ accumulators, offering a more detailed topographical overview of Aβ-dependent DMN changes. Our results expanded the body of literature regarding the association between Aβ deposition and aberrant DMN connectivity[17,67–73]—already described in populations with Alzheimer's dementia, mild cognitive impairment,[74–77] and subjective cognitive decline[78]—to cognitively healthy individuals with generally low amyloid burden. Moreover, we showed that localized Aβ accumulation in PCC has a synergistic effect with DMN connectivity in predicting longitudinal memory decline.

The mechanism through which Aβ deposition affects DMN connectivity remains still unclear. Pascoal *et al.* suggested that Aβ toxic effect is mediated by a local

Table 4 Voxel clusters that showed a significant association between amyloid burden (defined as Aβ 42/40 ratio and DVR in PCC) and FC and EC measures within the DMN

	Voxels	Brain area	Beta	Coordinate points			P-value
				x	y	z	
FC in DMN							
Aβ 42/40 ratio	423	Left cingulate gyrus	0.004	21	23	27	<0.001
	40	Right angular gyrus	0.004	31	15	26	<0.001
	12	Right precuneus	0.003	37	21	25	0.001
BP_{ND} in PCC	194	Left precuneus	−0.003	20	18	19	<0.001
	116	Left angular gyrus	−0.003	11	18	26	<0.001
	46	Right angular gyrus	−0.002	32	18	29	<0.001
	15	Left precuneus	−0.003	18	11	27	<0.001
EC in DMN							
Aβ 42/40 ratio	67	Left precuneus	0.004	17	16	26	<0.001
	40	Right precuneus	0.003	30	14	28	<0.001
	12	Right cingulate gyrus	0.003	22	24	26	0.001
	11	Right cingulate gyrus	0.003	25	20	27	0.002
	11	Left middle temporal gyrus	0.003	7	23	17	0.001
BP_{ND} in PCC	23	Right cingulate gyrus	−0.003	25	21	26	<0.001
	17	Left precuneus	−0.002	16	15	26	0.001
	15	Right angular gyrus	−0.002	31	18	27	<0.001

Models are corrected for age, sex, normalized GM volume and twin status. P-values are FWE-corrected.
Aβ, amyloid ß; BP_{ND}, non-displaceable binding potential; DMN, default-mode network; DVR, distribution volume ratio; FC, functional connectivity; FWE, family-wise error; PCC, posterior cingulate cortex; FWE, family-wise error.
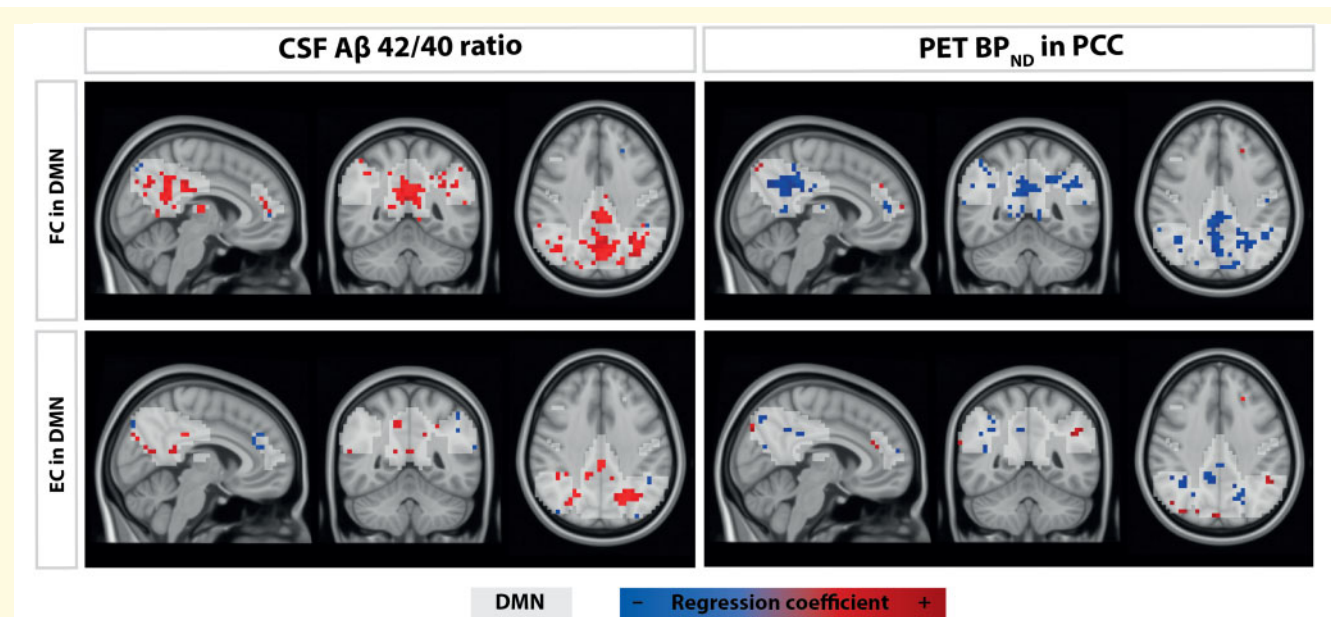
Figure 2. Results of voxelwise analyses. Aß, amyloid ß; DMN, default-mode network; DVR, distribution volume ratio; EC, eigenvector centrality; FC, functional connectivity; PCC, posterior cingulate cortex; PET, positron emission tomography.

Table 5 GEE linear mixed models predicting longitudinal memory decline

Predictor	Beta	*P*-value	Predictor	Beta	*P*-value
Two-way linear mixed model					
Aβ 42/40 ratio	−0.760	0.360	BP_{ND} in PCC	2.506	<0.001
Aβ 42/40 ratio*age	0.016	0.177	BP_{ND} in PCC*age	−0.041	<0.001
FC DMN	−1.556	0.021	FC DMN	0.187	0.846
FC DMN*age	0.0208	0.034	FC DMN*age	−0.006	<0.001
Three-way interaction model					
Aβ 42/40 ratio	−0.032	0.983	BP_{ND} in PCC	6.736	<0.001
FC DMN	−1.483	0.028	FC DMN	2.082	0.060
Aβ 42/40 ratio*age	0.005	0.825	BP_{ND} in PCC*age	−0.102	<0.001
Aβ 42/40 ratio*FC DMN	0.726	0.573	BP_{ND} in PCC*FC DMN	4.467	0.012
FC DMN*age	0.020	0.046	FC DMN*age	−0.034	0.039
Aβ 42/40 ratio*FC DMN*age	−0.011	0.551	BP_{ND} in PCC*FC DMN*age	−0.064	0.014

All models have been corrected for age at the time of examination, sex, and years of education and family ID was used as a random factor.
Aß, amyloid ß; DMN, default-mode network; DVR, distribution volume ratio; FC, functional connectivity; PCC, posterior cingulate cortex; GEE, generalized estimating equations.

reduction in metabolism in vulnerable neurons. The repercussions of such a phenomenon in the DMN can be *indirect*, affecting regions that are functionally connected with the DMN, or *direct*, if Aβ deposition topographically overlaps with DMN areas.[79] Metabolic stress might thus be the result of the large fluctuations of neuronal firing in these brain areas, which might be fueled by the toxic effect of Aβ and, on the other hand, could stimulate further Aβ accumulation through a positive feedback mechanism, eventually resulting in neuronal death.[80–83] The results of our voxelwise analyses provide evidence in support of the *direct* effect of Aβ plaques on neuronal metabolism, as FC and EC alterations in the DMN are associated with higher Aβ deposition in the PCC. This is in line with other studies showing topographical overlap

within the DMN regions of Aβ deposition, disrupted FC, hypometabolism, and atrophy in more advanced disease stages.[10,70,84–86]

Voxels that showed hypoconnectivity (as indicated by FC), higher sparsity and lower relative importance (as indicated by EC) of the DMN as a response to early-stage Aβ accumulation were localized in cingulate gyrus, angular gyrus, precuneus and middle temporal gyrus. Such regions demonstrate prominent atrophy in individuals further along the Alzheimer's disease continuum.[87] In particular, the PCC is an important hub of the medial temporal memory circuit, together with the hippocampus and enthorinal cortex.[88] Pathological and imaging studies have reported Aβ deposition, a lower number of synaptic connections, hypometabolic activity and lower FC in the

PCC of individuals with prodromal Alzheimer's disease and Alzheimer's dementia.[10,75,84,89,90] Our results confirm the central role of the PCC in Alzheimer's disease, further extending the concept to the earliest phases of $A\beta$ accumulation in cognitively healthy individuals,[8] as we show both early $A\beta$ deposition and aberrant connectivity in this area.

Not only do our findings indicate that DMN areas are vulnerable to Alzheimer's pathology, but they also suggest that DMN connectivity influences the rate of memory decline both independently and as a function of amyloid burden as measured with PET BP_{ND} in PCC. We did not find that DMN FC modified the association between CSF $A\beta$ 42/40 ratio and memory, possibly due to the different sensitivity of these measures.[4] Taken together, these findings suggest that the effect of early $A\beta$ accumulation on cognition might depend on neuronal vulnerability, which can in turn be quantified through FC and EC in the DMN. Our findings are in line with previous works in the literature, showing that amyloid-related alterations of brain FC appear before or together with cognitive alterations.[91] This could raise some questions regarding the definition of cognitively normal individuals in previous studies, as suggested by Brier *et al.*, but the discussion of this issue is beyond the scope of this study.[92]

The measures used for our analyses were defined based on different, possibly complementary, modalities. Specifically, amyloid burden was measured both through CSF ($A\beta$ 42/40 ratio) and amyloid PET (BP_{ND} in the PCC, precuneus, and MOF cortex) analyses. Similarly, we assessed DMN connectivity with two different measures, *i.e.* FC derived from ICA and EC. The definition of markers through multiple modalities ($A\beta$), different analytic techniques (rs-fMRI metrics), and composite scores (memory) and the inclusion of continuous biomarkers are methodological strengths of our study. Nevertheless, some methodological concerns should be addressed. Our sample is not totally representative of the general population, as it is mostly composed of highly educated white Caucasians, generally missing minorities. Moreover, our effect sizes were modest, probably due to the composition of our cohort, which was generally healthy and with a low amyloid burden, and to the fact that DMN FC and EC are indirect measures of brain hypometabolism. Still, we believe that this work shows strong evidence in support of the role of the DMN in $A\beta$-related changes, indicating that aberrant DMN connectivity likely mirrors early neurodegenerative processes.

In conclusion, we found that cognitively healthy individuals show disrupted connectivity and higher network disorganization and sparsity within the DMN as a function of incipient $A\beta$ accumulation. Moreover, FC within the DMN predicts longitudinal memory decline, suggesting that DMN connectivity might explain different trajectories of decline in individuals early along the Alzheimer's disease continuum, both independently of amyloid deposition and synergistically with regional amyloid deposition in the PCC. Taken together, these findings suggest that DMN plays an important role in early-stage Alzheimer's disease pathology, and consequently DMN connectivity is an interesting marker for the diagnostic and prognostic assessment of individuals in the earliest stages of Alzheimer's disease.

Acknowledgements

Funding

Conflict of interests

P.S. received grants from GE Healthcare, Piramal and Merck, paid to his institution; he has received speaker's fees paid to the institution Alzheimer Center, VU University Medical Center, Lilly, GE Healthcare, and Roche. B.N.M.v.B. received research support from ZON-MW, AVID radiopharmaceuticals, CTMM and Janssen

References

1. Jansen WJ, Ossenkoppele R, Tijms BM, et al. Amyloid Biomarker Study Group. Association of cerebral amyloid-β aggregation with cognitive functioning in persons without dementia. *JAMA Psychiatry*. 2018;75(1):84–95.

2. Morris J, Roe C, Grant E, et al. Pittsburgh compound b imaging and prediction of progression from cognitive normality to symptomatic Alzheimer disease. *Arch Neurol*. 2009;66(12):1469–1475.

3. ten Kate M, Ingala S, Schwarz AJ, et al. Secondary prevention of Alzheimer's dementia: Neuroimaging contributions. *Alzheimers Res Ther*. 2018;10(1):112.

4. Palmqvist S, Mattsson N, Hansson O; for the Alzheimer's Disease Neuroimaging Initiative. Cerebrospinal fluid analysis detects cerebral amyloid-β accumulation earlier than positron emission tomography. *Brain*. 2016;139(4):1226–1236.

5. Parihar MS, Brewer GJ. Amyloid-β as a modulator of synaptic plasticity. *J Alzheimer's Dis*. 2010;22(3):741–763.

6. Park J, Jang M, Chang S. Deleterious effects of soluble amyloid-β oligomers on multiple steps of synaptic vesicle trafficking. *Neurobiol Dis*. 2013;55:129–139.

7. Grothe MJ, Barthel H, Sepulcre J, Dyrba M, Sabri O, Teipel SJ; Alzheimer's Disease Neuroimaging Initiative. In vivo staging of regional amyloid deposition. *Neurology*. 2017;89(20):2031–2038.

8. Collij LE, Heeman F, Salvadó G, et al.; on behalf of the AMYPAD Consortium. Multitracer model for staging cortical amyloid deposition using PET imaging. *Neurology*. 2020;95(11):e1538–e1553.

9. Palmqvist S, Schöll M, Strandberg O, et al. Earliest accumulation of β-amyloid occurs within the default-mode network and concurrently affects brain connectivity. *Nat Commun*. 2017;8(1):1214.

10. Buckner RL, Snyder AZ, Shannon BJ, et al. Molecular, structural, and functional characterization of Alzheimer's disease: evidence for a relationship between default activity, amyloid, and memory. *J Neurosci*. 2005;25(34):7709–7717.

11. Sperling RA, Laviolette PS, O'Keefe K, et al. Amyloid deposition is associated with impaired default network function in older persons without dementia. *Neuron*. 2009;63(2):178–188.

12. Sepulcre J, Sabuncu MR, Becker A, Sperling R, Johnson KA. In vivo characterization of the early states of the amyloid-beta network. *Brain*. 2013;136 (Pt 7):2239–2252.

13. Myers N, Pasquini L, Göttler J, et al. Within-patient correspondence of amyloid-β and intrinsic network connectivity in Alzheimer's disease. *Brain*. 2014;137 (Pt 7):2052–2064.

14. Barkhof F, Haller S, Rombouts SARB. Resting-state functional MR imaging: A new window to the brain. *Radiology*. 2014;272(1):29–49.

15. Staffaroni AM, Brown JA, Casaletto KB, et al. The longitudinal trajectory of default mode network connectivity in healthy older adults varies as a function of age and is associated with changes in episodic memory and processing speed. *J Neurosci*. 2018;38(11):2809–2817.

16. Desgranges B, Mevel K, Chételat G, Eustache F. The default mode network in healthy aging and Alzheimer's disease. *Int J Alzheimers Dis*. 2011;2011:535816.

17. Elman JA, Madison CM, Baker SL, et al. Effects of beta-amyloid on resting state functional connectivity within and between networks reflect known patterns of regional vulnerability. *Cereb Cortex*. 2014;26(2):695–707.

18. Buckner RL. The serendipitous discovery of the brain's default network. *Neuroimage*. 2012;62(2):1137–1145.

19. Buckner RL, Andrews-Hanna JR, Schacter DL. The brain's default network: Anatomy, function, and relevance to disease. *Ann N Y Acad Sci*. 2008;1124:1–38.

20. Wink AM, Tijms BM, ten Kate M, et al. Functional brain network centrality is related to APOE genotype in cognitively normal elderly. *Brain Behav*. 2018;8(9):e01080.

21. Filippini N, MacIntosh BJ, G. Houghb M, et al. Distinct patterns of brain activity in young carriers of the APOE-4 allele. *Proc Natl Acad Sci USA*. 2009;106(17):7209–7214.

22. van den Heuvel MP, Hulshoff Pol HE. Exploring the brain network: A review on resting-state fMRI functional connectivity. *Eur Neuropsychopharmacol*. 2010;20(8):519–534.

23. Wang J, Zuo X, He Y. Graph-based network analysis of resting-state functional MRI. *Front Syst Neurosci*. 2010;4:16.

24. Wink AM, de Munck JC, Van Der Werf YD, Van Den Heuvel OA, Barkhof F. Fast eigenvector centrality mapping of voxel-wise connectivity in functional magnetic resonance imaging: Implementation, validation, and interpretation. *Brain Connect*. 2012;2(5):265–274.

25. Binnewijzend MAA, Adriaanse SM, Van der Flier WM, et al. Brain network alterations in Alzheimer's disease measured by Eigenvector centrality in fMRI are related to cognition and CSF biomarkers. *Hum Brain Mapp*. 2014;35(5):2383–2393.

26. Binder JR, Frost JA, Hammeke TA, Bellgowan PSF, Rao SM, Cox RW. Conceptual Processing during the Conscious Resting State: A Functional MRI Study. *J Cogn Neurosci*. 1999;11(1):80–93.

27. Jahn H. Memory loss in Alzheimer's disease. *Dialogues Clin Neurosci*. 2013;15(4):445–454.

28. Ritchie K, Ropacki M, Albala B, et al. Recommended cognitive outcomes in preclinical Alzheimer's disease: Consensus statement from the European Prevention of Alzheimer's Dementia project. *Alzheimer's Dement*. 2017;13(2):186–195.

29. Konijnenberg E, den Braber A, ten Kate M, et al. Association of amyloid pathology with memory performance and cognitive complaints in cognitively normal older adults: A monozygotic twin study. *Neurobiol Aging*. 2019;77:58–65.

30. Jack C, Wiste HJ, Vemuri P, et al.; Alzheimer's Disease Neuroimaging Initiative. Brain beta-amyloid measures and magnetic resonance imaging atrophy both predict time-to-progression from mild cognitive impairment to Alzheimer's disease. *Brain*. 2010;133(11):3336–3348.

31. Vemuri P, Wiste HJ, Weigand SD, et al.; Alzheimer's Disease Neuroimaging Initiative. MRI and CSF biomarkers in normal, MCI, and AD subjects: Predicting future clinical change. *Neurology*. 2009;73(4):294–301.

32. Konijnenberg E, Carter SF, Ten Kate M, et al. The EMIF-AD PreclinAD study: Study design and baseline cohort overview. *Alzheimer's Res Ther*. 2018;10(1):75.

33. Morris JC, Edland S, Clark C, et al. The consortium to establish a registry for Alzheimer's disease (CERAD). Part IV. Rates of

cognitive change in the longitudinal assessment of probable Alzheimer's disease. *Neurology*. 1993;43(12):2457–2465.

34. De Jager CA, Budge MM, Clarke R. Utility of TICS-M for the assessment of cognitive function in older adults. *Int J Geriatr Psychiatry*. 2003;18(4):318–324.

35. Yesavage JA, Brink TL, Rose TL, et al. Development and validation of a geriatric depression screening scale: A preliminary report. *J Psychiatr Res*. 1982;17(1):37–49.

36. Morris JC. The clinical dementia rating (CDR). Neurology. 1993; 43(11):2412–2414.

37. Rey A. L'examen clinique en psychologie. Presses universitaires de France; 1964;95.

38. Tolboom N, Van Der Flier WM, Yaqub M, et al. Differential association of [11C]PIB and [18F]FDDNP binding with cognitive impairment. *Neurology*. 2009;73(24):2079–2085.

39. Meyers JE, Bayless JD, Meyers KR. Rey complex figure: Memory error patterns and functional abilities. *Appl Neuropsychol*. 1996; 3(2):89–92.

40. Snitz BE, Weissfeld LA, Lopez OL, et al. Cognitive trajectories associated with β-amyloid deposition in the oldest-old without dementia. *Neurology*. 2013;80(15):1378–1384.

41. Rentz DM, Amariglio RE, Becker JA, et al. Face-name associative memory performance is related to amyloid burden in normal elderly. *Neuropsychologia*. 2011;49(9):2776–2783.

42. Papp KV, Amariglio RE, Dekhtyar M, et al. Development of a psychometrically equivalent short form of the Face-Name Associative Memory Exam for use along the early Alzheimer's disease trajectory NIH Public Access. *Clin Neuropsychol*. 2014;28(5):771–785.

43. del Campo M, Mollenhauer B, Bertolotto A, et al. Recommendations to standardize preanalytical confounding factors in Alzheimer's and Parkinson's disease cerebrospinal fluid biomarkers: An update. *Biomark Med*. 2012;6(4):419–430.

44. De Vos A, Jacobs D, Struyfs H, et al. C-terminal neurogranin is increased in cerebrospinal fluid but unchanged in plasma in Alzheimer's disease. *Alzheimer's Dement*. 2015;11(12):1461–1469.

45. Janelidze S, Pannee J, Mikulskis A, et al. Concordance between different amyloid immunoassays and visual amyloid positron emission tomographic assessment. *JAMA Neurol*. 2017;74(12):1492–1501.

46. Heeman F, Yaqub M, Lopes Alves I, et al.; AMYPAD Consortium. Optimized dual-time-window protocols for quantitative [18F]flutemetamol and [18F]florbetaben PET studies. *EJNMMI Res*. 2019;9(1):32.

47. Smith SM, Zhang Y, Jenkinson M, et al. Accurate, robust, and automated longitudinal and cross-sectional brain change analysis. *Neuroimage*. 2002;17(1):479–489.

48. Smith SM, Jenkinson M, Woolrich MW, et al. Advances in functional and structural MR image analysis and implementation as FSL. *Neuroimage*. 2004;23 (Suppl 1):S208–S219.

49. Jenkinson M, Bannister P, Brady M, Smith S. Improved optimization for the robust and accurate linear registration and motion correction of brain images. *Neuroimage*. 2002;17(2):825–841.

50. Smith SM. Fast robust automated brain extraction. *Hum Brain Mapp*. 2002;17(3):143–155.

51. Popescu V, Battaglini M, Hoogstrate WS, et al.; MAGNIMS Study Group. Optimizing parameter choice for FSL-Brain Extraction Tool (BET) on 3D T1 images in multiple sclerosis. *Neuroimage*. 2012;61(4):1484–1494.

52. Beckmann CF, DeLuca M, Devlin JT, Smith SM. Investigations into resting-state connectivity using independent component analysis. *Philos Trans R Soc B Biol Sci*. 2005;360(1457): 1001–1013.

53. Smith SM, Fox PT, Miller KL, et al. Correspondence of the brain's functional architecture during activation and rest. *Proc Natl Acad Sci*. 2009;106(31):13040–13045.

54. Beckmann C, Mackay C, Filippini N, Smith S. Group comparison of resting-state FMRI data using multi-subject ICA and dual regression. *Neuroimage*. 2009;47 (Suppl 1):S148.

55. Nickerson LD, Smith SM, Öngür D, Beckmann CF. Using dual regression to investigate network shape and amplitude in functional connectivity analyses. *Front Neurosci*. 2017;11:115.

56. Smith DV, Utevsky AV, Bland AR, et al. Characterizing individual differences in functional connectivity using dual-regression and seed-based approaches. *Neuroimage*. 2014;95:1–12.

57. Wink AM. Eigenvector centrality dynamics from resting-state fMRI: Gender and age differences in healthy subjects. *Front Neurosci*. 2019;13:648.

58. Lohmann G, Margulies DS, Horstmann A, et al. Eigenvector centrality mapping for analyzing connectivity patterns in fMRI data of the human brain. *PLoS One*. 2010;5(4):e10232.

59. Hammers A, Allom R, Koepp MJ, et al. Three-dimensional maximum probability atlas of the human brain, with particular reference to the temporal lobe. *Hum Brain Mapp*. 2003;19(4): 224–247.

60. Svarer C, Madsen K, Hasselbalch SG, et al. MR-based automatic delineation of volumes of interest in human brain PET images using probability maps. *Neuroimage*. 2005;24(4):969–979.

61. Lammertsma AA, Hume SP. Simplified reference tissue model for PET receptor studies. Neuroimage. 1996;4 (3 Pt 1):153–158.

62. Boellaard R, Yaqub M, Lubberink M, Lammertsma A. PPET: A software tool for kinetic and parametric analyses of dynamic PET studies. *Neuroimage*. 2006;31:T62.

63. Desikan RS, Ségonne F, Fischl B, et al. An automated labeling system for subdividing the human cerebral cortex on MRI scans into gyral based regions of interest. *Neuroimage*. 2006;31(3):968–980.

64. Minică CC, Dolan CV, Kampert MMD, Boomsma DI, Vink JM. Sandwich corrected standard errors in family-based genome-wide association studies. *Eur J Hum Genet*. 2015;23(3):388–394.

65. Landau SM, Horng A, Jagust WJ; Alzheimer's Disease Neuroimaging Initiative. Memory decline accompanies subthreshold amyloid accumulation. *Neurology*. 2018;90(17): E1452–E1460.

66. Wirth M, Oh H, Mormino EC, Markley C, Landau SM, Jagust WJ. The effect of amyloid β on cognitive decline is modulated by neural integrity in cognitively normal elderly. *Alzheimer's Dement*. 2013;9(6):687–698.e1.

67. Hedden T, Van Dijk KRA, Becker JA, et al. Disruption of functional connectivity in clinically normal older adults harboring amyloid burden. *J Neurosci*. 2009;29(40):12686–12694.

68. Mormino EC, Smiljic A, Hayenga AO, et al. Relationships between beta-amyloid and functional connectivity in different components of the default mode network in aging. *Cereb Cortex*. 2011;21(10):2399–2407.

69. Oh H, Mormino EC, Madison C, Hayenga A, Smiljic A, Jagust WJ. β-Amyloid affects frontal and posterior brain networks in normal aging. *Neuroimage*. 2011;54(3):1887–1895.

70. Drzezga A, Becker JA, Van Dijk KRA, et al. Neuronal dysfunction and disconnection of cortical hubs in non-demented subjects with elevated amyloid burden. *Brain*. 2011;134 (Pt 6):1635–1646.

71. Brier MR, Thomas JB, Fagan AM, et al. Functional connectivity and graph theory in preclinical Alzheimer's disease. *Neurobiol Aging*. 2014;35(4):757–768.

72. Wang L, Brier MR, Snyder AZ, et al. Cerebrospinal fluid Aβ42, phosphorylated Tau181, and resting-state functional connectivity. *JAMA Neurol*. 2013;70(10):1242–1248.

73. Sheline YI, Raichle ME. Resting state functional connectivity in preclinical Alzheimer's disease. *Biol Psychiatry*. 2013;74(5): 340–347.

74. Bai F, Zhang Z, Yu H, et al. Default-mode network activity distinguishes amnestic type mild cognitive impairment from healthy aging: A combined structural and resting-state functional MRI study. *Neurosci Lett*. 2008;438(1):111–115.

75. Greicius MD, Srivastava G, Reiss AL, Menon V. Default-mode network activity distinguishes Alzheimer's disease from healthy aging: Evidence from functional MRI. *Proc Natl Acad Sci U S A*. 2004;101(13):4637–4642.

76. Rombouts SARB, Barkhof F, Goekoop R, Stam CJ, Scheltens P. Altered resting state networks in mild cognitive impairment and mild Alzheimer's disease: An fMRI study. *Hum Brain Mapp*. 2005;26(4):231–239.

77. Sorg C, Riedl V, Mühlau M, et al. Selective changes of resting-state networks in individuals at risk for Alzheimer's disease. *Proc Natl Acad Sci U S A*. 2007;104(47):18760–18765.

78. Verfaillie SCJ, Pichet Binette A, Vachon-Presseau E, et al. Subjective cognitive decline is associated with altered default mode network connectivity in individuals with a family history of Alzheimer's disease. *Biol Psychiatry Cogn Neurosci Neuroimaging*. 2018;3(5): 463–472.

79. Pascoal TA, Mathotaarachchi S, Kang MS, et al. Aβ-induced vulnerability propagates via the brain's default mode network. *Nat Commun*. 2019;10(1):2353–2313.

80. Cirrito JR, Kang JE, Lee J, et al. Endocytosis is required for synaptic activity-dependent release of amyloid-β in vivo. *Neuron*. 2008; 58(1):42–51.

81. Kamenetz F, Tomita T, Hsieh H, et al. APP processing and synaptic function. *Neuron*. 2003;37(6):925–937.

82. Klebanoff C. A, Khong HT, Antony P. A, Palmer DC, Restifo NP. Sinks, suppressors and antigen presenters: How lymphodepletion enhances T cell-mediated tumor immunotherapy. *Trends Immunol*. 2005;26(2):111–117.

83. Li X, Uemura K, Hashimoto T, et al. Neuronal activity and secreted amyloid β lead to altered amyloid β precursor protein and presenilin 1 interactions. *Neurobiol Dis*. 2013;50(1): 127–134.

84. Minoshima S, Giordani B, Berent S, Frey KA, Foster NL, Kuhl DE. Metabolic reduction in the posterior cingulate cortex in very early Alzheimer's disease. *Ann Neurol*. 1997;42(1):85–94.

85. Mosconi L, De Santi S, Li J, et al. Hippocampal hypometabolism predicts cognitive decline from normal aging. *Neurobiol Aging*. 2008;29(5):676–692.

86. Scahill RI, Schott JM, Stevens JM, Rossor MN, Fox NC. Mapping the evolution of regional atrophy in Alzheimer's disease: Unbiased analysis of fluid-registered serial MRI. *Proc Natl Acad Sci U S A*. 2002;99(7):4703–4707.

87. Bailly M, Destrieux C, Hommet C, et al. Precuneus and cingulate cortex atrophy and hypometabolism in patients with Alzheimer's disease and mild cognitive impairment: MRI and ^{18}F-FDG PET quantitative analysis using FreeSurfer. *Biomed Res Int*. 2015;2015:1–8.

88. Leech R, Sharp DJ. The role of the posterior cingulate cortex in cognition and disease. *Brain*. 2014;137 (Pt 1):12–32.

89. Scheff SW, Price DA, Ansari MA, et al. Synaptic change in the posterior cingulate gyrus in the progression of Alzheimer's disease NIH public access. *J Alzheimers Dis*. 2015;43(3):1073–1090.

90. Johnson KA, Jones K, Holman BL, et al. Preclinical prediction of Alzheimer's disease using SPECT. *Neurology*. 1998;50(6): 1563–1571.

91. Sheline YI, Raichle ME, Snyder AZ, et al. Amyloid plaques disrupt resting state default mode network connectivity in cognitively normal elderly. *Biol Psychiatry*. 2010;67(6):584–587.

92. Brier MR, Thomas JB, Snyder AZ, et al. Unrecognized preclinical Alzheimer disease confounds rs-fcMRI studies of normal aging. *Neurology*. 2014;83(18):1613–1619.